Journal of Solid State Chemistry 184 (2011) 2360–2367

Contents lists available at ScienceDirect

Journal of Solid State Chemistry

journal homepage: www.elsevier.com/locate/jssc

Ternary rare-earth zinc arsenides $RE\mathrm{Zn}_{1-x}\mathrm{As}_2$ (RE=La–Nd, Sm)

Stanislav S. Stoyko, Arthur Mar*

Department of Chemistry, University of Alberta, Edmonton, Alberta, Canada T6G 2G2

ARTICLE INFO

Article history:
Received 18 May 2011
Received in revised form
29 June 2011
Accepted 2 July 2011
Available online 13 July 2011

Keywords:
Rare earths
Arsenides
Crystal structure
Electronic structure
Magnetic properties

ABSTRACT

The ternary rare-earth zinc arsenides $RE\mathrm{Zn}_{1-x}\mathrm{As}_2$ (RE=La–Nd, Sm) were prepared by reaction of the elements at 800 °C. Single-crystal and powder X-ray diffraction analysis revealed a defect SrZnBi_2-type average structure for the La member (Pearson symbol $tI16$, space group $I4/mmm$, $Z=4$; $a=4.0770(9)$ Å, $c=20.533(5)$ Å), in contrast to defect HfCuSi_2-type average structures for the remaining RE members (Pearson symbol $tP8$, space group $P4/nmm$, $Z=2$; $a=4.0298(5)$–$3.9520(4)$ Å, $c=10.222(1)$–$10.099(1)$ Å in the progression from Ce to Sm). The homogeneity range is not appreciable (estimated to be narrower than $0.6<1-x<0.7$ in $\mathrm{SmZn}_{1-x}\mathrm{As}_2$) and the formula $RE\mathrm{Zn}_{0.67}\mathrm{As}_2$ likely represents the Zn-rich phase boundary. The Ce–Nd members are Curie–Weiss paramagnets. $\mathrm{LaZn}_{0.67}\mathrm{As}_2$ shows activated behavior in its electrical resistivity, whereas $\mathrm{SmZn}_{0.67}\mathrm{As}_2$ exhibits anomalies in its temperature dependence of the electrical resistivity.

1. Introduction

The most prevalent ternary rare-earth transition-metal pnictides have the ideal general composition $REMPn_2$. They typically adopt the HfCuSi_2-type structure [1], an important type that has gained prominence in recent years because of its close connection to the many superconducting quaternary pnictide oxides now in vogue [2]. However, many of the ternary pnictides themselves are interesting in their own right, prone to structural distortions and exhibiting exotic physical properties. Ternary antimonides are known for a wide range of transition metals ($REMSb_2$; M=Mn, Fe, Co, Ni, Pd, Cu, Ag, Au, Zn, Cd) [3], whereas bismuthides ($REMBi_2$; M=Ni, Cu, Ag, Zn) [4] and arsenides ($REMAs_2$; M=Cu, Ag, Au, Zn) [5–9] are still relatively limited. The square nets of Pn atoms present in the structures of these compounds are subject to Peierls instabilities, leading to lowering of symmetry and the appearance of commensurately or even incommensurately modulated superstructures [9–15]. A deficiency of the transition-metal component frequently occurs, corresponding to the formula $REM_{1-x}Pn_2$, but an excess can also be observed, as in $RE\mathrm{Cu}_{1+x}\mathrm{As}_2$ [16,17]. The arsenides $REMAs_2$ (M=Cu, Ag, Au) have been highlighted for their anomalous transport and magnetic properties [15,18–22].

Among the Zn-containing series, the extent of RE substitution has been elucidated and property measurements have been made previously for the antimonides ($RE\mathrm{Zn}_{1-x}\mathrm{Sb}_2$; RE=La–Nd, Sm, Gd, Tb) [23] and bismuthides ($RE\mathrm{Zn}_{1-x}\mathrm{Bi}_2$; RE=La, Ce, Pr) [24], whereas the crystal structure of $\mathrm{PrZn}_{0.67}\mathrm{As}_2$ (which demonstrates an interesting vacancy ordering) is the only information available so far for the arsenides $RE\mathrm{Zn}_{1-x}\mathrm{As}_2$ [6]. We report here a systematic investigation of the $RE\mathrm{Zn}_{1-x}\mathrm{As}_2$ series, presenting crystallographic analyses, measurements of electrical and magnetic properties, and electronic structure calculations.

2. Experimental

2.1. Synthesis

Starting materials were freshly filed RE pieces (99.9%, Hefa), Zn shot (99.99%, Aldrich), and As lumps (99.999%, Alfa-Aesar). Mixtures of RE, Zn, and As in the molar ratio 1:0.67:2 on a 0.3-g scale were placed within sealed evacuated fused-silica tubes. The tubes were heated at 500 °C for 48 h, heated to 800 °C over 24 h, held at that temperature for 96 h, and then cooled to room temperature over 48 h. The as-prepared samples were reground and further annealed at 800 °C for 240 h. Powder X-ray diffraction (XRD) patterns, collected on an Inel powder diffractometer (Cu $K\alpha_1$ radiation) equipped with a CPS 120 detector, were examined to assess product purity (Fig. S1 in Supplementary Data) and to determine refined cell parameters (Table 1). Single-phase products of $RE\mathrm{Zn}_{0.67}\mathrm{As}_2$ were obtained for RE=La–Nd, Sm; attempts to extend the RE substitution to the heavier members (Gd–Er) under similar synthesis conditions were unsuccessful, with binary RE–As and Zn–As phases being formed instead.

Single crystals of $RE\mathrm{Zn}_{0.67}\mathrm{As}_2$ were grown by placing phase-pure powder samples, obtained above, in alumina crucibles within sealed evacuated fused-silica tubes, which were heated

* Corresponding author. Fax: +1 780 492 8231.
E-mail address: arthur.mar@ualberta.ca (A. Mar).

0022-4596/$ - see front matter © 2011 Elsevier Inc. All rights reserved.
doi:10.1016/j.jssc.2011.07.002

at 900 °C for 96 h, cooled to 800 °C over 48 h, and held at that temperature for 240 h, either with the addition of a few mg of I_2 as a mineralizing agent (for RE=La–Nd) or without it (for RE=Sm). Energy-dispersive X-ray (EDX) analysis with a Hitachi S-2700 scanning electron microscope on these crystals showed the presence of all three elements in ratios (Table 2) that are consistent with the formulas obtained from the structure determinations.

Further reactions with loading compositions $SmZn_{0.60}As_2$, $SmZn_{0.65}As_2$, and $SmZn_{0.70}As_2$ were conducted to establish the homogeneity range, if any. The desired ternary $HfCuSi_2$-type phase was found as the major product in all cases but the $SmZn_{0.60}As_2$ sample also contained SmAs whereas the $SmZn_{0.70}As_2$ sample contained SmAs and another ternary phase ($SmZn_3As_3$) [25]. Cell parameters refined for the $HfCuSi_2$-type phase in these three samples are identical within a 3σ-threshold (a=3.9503(6)–3.9522(8) Å, c=10.092(2)–10.098(2) Å, V=157.48(5)–157.70(5) Å^3 if the tetragonal subcell is assumed), implying that the homogeneity range is negligible and that the Zn deficiency is essentially fixed.

Table 1
Cell parameters for $RE Zn_{1-x}As_2$[a].

Compound	a (Å)	c (Å)	V/Z (Å^3)
$LaZn_{0.67}As_2$	4.0747(6)	20.524(3)	85.19(2)
$CeZn_{0.67}As_2$	4.0298(5)	10.222(1)	83.00(2)
$PrZn_{0.67}As_2$[b]	4.0100(9)	10.202(4)	82.02(4)
$NdZn_{0.67}As_2$	3.9890(6)	10.163(2)	80.86(2)
$SmZn_{0.67}As_2$	3.9522(8)	10.095(2)	78.84(3)

[a] Refined from powder X-ray diffraction data.
[b] For comparison, cell parameters from single-crystal data are a=4.006(1) Å and c=10.197(4) Å [6].

Table 2
EDX analyses of $RE Zn_{1-x}As_2$ crystals[a].

Compound	at% RE	at% Zn	at% As
$LaZn_{0.67}As_2$	28(1)	19(1)	53(2)
$CeZn_{0.67}As_2$	29(2)	18(1)	53(2)
$PrZn_{0.67}As_2$	30(1)	18(1)	52(1)
$NdZn_{0.67}As_2$	29(1)	18(1)	53(1)
$SmZn_{0.67}As_2$	30(1)	18(1)	52(1)

[a] Averaged over ~10 crystals per compound.

2.2. Structure determination

Single-crystal intensity data for $LaZn_{0.67}As_2$ and $SmZn_{0.67}As_2$ were collected on a Bruker D8/SMART APEX II CCD diffractometer at 22 °C using ω scans. Structure solution and refinement were carried out with use of the SHELXTL (version 6.12) program package [26]. Face-indexed numerical absorption corrections were applied. Crystal data and further details of the data collection are given in Table 3.

For $LaZn_{0.67}As_2$, the centrosymmetric space group $I4/mmm$ was chosen on the basis of Laue symmetry and systematic absences. Direct methods revealed a $SrZnBi_2$-type structure [27] and refinements proceeded in a straightforward manner, with the occupancy of the Zn site (4d) converging to 0.663(5), in good agreement with the nominal composition used in the synthesis. The displacement ellipsoid of the As2 site (4c) is slightly extended along the a-direction (U_{11}=0.0461(7) Å^2; U_{eq}=0.0240(3) Å^2), though not as extreme as in the previously reported case of $LaAuAs_2$ (U_{11}=0.0987(4) Å^2; U_{eq}=0.0462(13) Å^2) [9]. A split model analogous to that proposed for $LaAuAs_2$ was applied [9], in which As2 atoms were placed in a 16l site and refined isotropically, resulting in U_{iso}=0.0122(4) Å^2 for a site located at (0.0407(4), 0.4869(15), 0) with a slightly greater conventional residual of R=0.020. Given the prolate shape of the As2 displacement ellipsoid in the unsplit model, another possibility was considered in which the mirror symmetry of the As2 atoms is retained by placing them in a 8j site (0.0402(4), 1/2, 0), resulting

Table 3
Crystallographic data for $LaZn_{1-x}As_2$ and $SmZn_{1-x}As_2$.

Formula	$LaZn_{0.663(5)}As_2$	$SmZn_{0.641(3)}As_2$
Formula mass (amu)	332.06	342.03
Space group	$I4/mmm$ (no. 139)	$P4/nmm$ (no. 129)
a (Å)	4.0770(9)	3.9520(4)
c (Å)	20.533(5)	10.0993(10)
V (Å^3)	341.30(13)	157.73(3)
Z	4	2
ρ_{calcd} (g cm^{-3})	6.462	7.201
Crystal dimensions (mm)	0.12 × 0.08 × 0.02	0.20 × 0.08 × 0.04
Radiation	Graphite monochromated Mo $K\alpha$, λ=0.71073 Å	
μ(Mo $K\alpha$) (mm^{-1})	36.01	43.86
Transmission factors	0.104–0.590	0.042–0.240
2θ limits	$3.96° \le 2\theta(\text{Mo } K\alpha) \le 65.68°$	$4.04° \le 2\theta(\text{Mo } K\alpha) \le 65.84°$
Data collected	$-6 \le h \le 6$ $-6 \le k \le 6$ $-30 \le l \le 30$	$-5 \le h \le 5$ $-6 \le k \le 5$ $-15 \le l \le 14$
No. of data collected	2246	2102
No. of unique data, including $F_o^2 < 0$	233 (R_{int}=0.041)	218 (R_{int}=0.025)
No. of unique data, with $F_o^2 > 2\sigma(F_o^2)$	205	217
No. of variables	14	13
$R(F)$ for $F_o^2 > 2\sigma(F_o^2)$[a]	0.018	0.015
$R_w(F_o^2)$[b]	0.045	0.034
Goodness of fit	1.23	1.29
$(\Delta\rho)_{max}$, $(\Delta\rho)_{min}$ (e Å^{-3})	0.90, −1.04	1.03, −2.55

[a] $R(F) = \sum \| F_o | - | F_c \| / \sum | F_o |$.

[b] $R_w(F_o^2) = \left[\sum [w(F_o^2 - F_c^2)^2] / \sum w F_o^4 \right]^{1/2}$; $w^{-1} = [\sigma^2(F_o^2) + (Ap)^2 + Bp]$ where $p = [\max(F_o^2, 0) + 2F_c^2]/3$

in $U_{iso}=0.0133(3)$ Å^2 and $R=0.020$. (A comparison of interatomic distances generated within the square net of As2 atoms in the unsplit vs. split models is shown in Fig. S2 in Supplementary Data.) We have opted to retain the model with the unsplit As2 site, recognizing that this likely represents an average structure; the elevated displacement parameters are typical for this site, but in this case, whatever distortion that arises will be small and probably difficult to detect in a superstructure. Inspection of the powder XRD pattern (Fig. S1(a) in Supplementary Data) reveals no obvious peak splitting that would suggest a transformation to a lower lattice symmetry.

For $SmZn_{0.67}As_2$, a structural model was developed in the centrosymmetric space group *P*4/*nmm*, with initial atomic positions taken from the previously reported subcell of $Pr_3Zn_2As_6$ [6], which adopts a defect $HfCuSi_2$-type structure. Refinement of this model revealed full occupancy and acceptable displacement parameters for all sites, except for the Zn site (2*b*). When allowed to refine freely, the occupancy of this site converged to 0.641(3) and the displacement parameters were reduced to reasonable values. Being aware of the possibility of twinning as well as the reported superstructure of $Pr_3Zn_2As_6$ (in the orthorhombic space group *Pmmn*, with $a'=a$, $b'=3a$, and $c'=c$, showing ordering of a vacant Zn site) [6], we attempted to elaborate on these models too, with the use of the program CELL_NOW [28] to separate the raw data set into two twin domains in accordance with the transformation to the larger unit cell. However, these refinements revealed substantial residual electron density at the location of the vacant Zn site in the $1\times3\times1$ superstructure model. Such an ordering could not be established even after additional annealing of the $SmZn_{0.67}As_2$ single crystals at 800 °C for a further 10 *d*. There is evidence for the existence of a different, more complex superstructure, as revealed by inspection of the *hk*0 layer of reflections in the CCD frames for the original data set (Fig. S3 in Supplementary Data), that needs to be analyzed in more detail. Attempts to resolve this superstructure, which poses a challenging problem, are in progress. Although the powder XRD patterns for $REZn_{0.67}As_2$ (*RE*=Ce–Nd, Sm) do suggest a lowering of tetragonal to orthorhombic symmetry, the extent of peak splitting depends on the *RE* substitution and is not evident at all for the Nd member (Fig. S1 in Supplementary Data). It is thus likely that the superstructure found in $Pr_3Zn_2As_6$ may not necessarily be valid for other *RE* members of $REZn_{0.67}As_2$. In the discussion below, we report results based on the subcell model, on the understanding that this represents only an average structure.

Atomic positions were standardized with the program STRUCTURE TIDY [29]. Final values of the positional and displacement parameters are given in Table 4 and selected interatomic distances are given in Table 5. Further data, in CIF format, have been sent to Fachinformationszentrum Karlsruhe, Abt. PROKA, 76344 Eggenstein-Leopoldshafen, Germany, as supplementary material nos. CSD-423247 and -423248 and can be obtained by contacting FIZ (quoting the article details and the corresponding CSD numbers).

2.3. Band structure calculations

Tight-binding linear muffin tin orbital (TB-LMTO) band structure calculations were performed on a "$LaZnAs_2$" model ($SrZnBi_2$-type structure) with hypothetically full Zn occupancies and structural parameters taken from the single-crystal X-ray diffraction studies, within the local density and atomic spheres approximation with use of the Stuttgart TB-LMTO program [30]. The basis sets consisted of La 6*s*/6*p*/5*d*/4*f*, Zn 4*s*/4*p*/3*d*, and As 4*s*/4*p*/4*d* orbitals, with the La 6*p* and As 4*d* orbitals being downfolded. Integrations in reciprocal space were carried out with an improved tetrahedron method over 59 irreducible *k* points within the first Brillouin zone for $LaZnAs_2$.

2.4. Physical property measurements

Plate-shaped single crystals of $LaZn_{0.67}As_2$ and $SmZn_{0.67}As_2$, whose identities were verified by EDX analysis, were sufficiently large (0.4 mm in their longest dimensions) to permit electrical resistivity measurements, which were made between 2 and 300 K by standard four-probe techniques on a Quantum Design Physical Property Measurement System (PPMS) equipped with an alternating current (ac) transport controller (model 7100). Silver paste was used as the contacting agent between gold wires, graphite fibers, and single crystals. The current was 100 μA and the frequency was 16 Hz. Given the crystal habit, the resistivity could be measured only within the plane of the platelets, which corresponds to the crystallographic *ab*-plane. All measurements were performed at least twice.

Measurements of direct current (dc) magnetic susceptibility were made on powders of $REZn_{0.67}As_2$ (*RE*=Ce, Pr, and Nd) between 2 and 300 K under an applied field of 0.5 T on a Quantum

Table 5
Selected interatomic distances (Å) in $LaZn_{1-x}As_2$ and $SmZn_{1-x}As_2$.

	$LaZn_{0.663(5)}As_2$	$SmZn_{0.641(3)}As_2$
RE–As1 (× 4)	3.1358(7)	3.0156(4)
RE–As2 (× 4)	3.1080(6)	3.0373(3)
RE–Zn (× 4)	3.4532(7)	3.3806(3)
Zn–As1 (× 4)	2.5629(7)	2.5486(4)
Zn–Zn (× 4)	2.8829(6)	2.7945(3)
As2–As2 (× 4)	2.8829(6)	2.7945(3)

Table 4
Positional and displacement parameters for $LaZn_{1-x}As_2$ and $SmZn_{1-x}As_2$.

Atom	Wyckoff position	*x*	*y*	*z*	U_{11} (Å^2)	U_{22} (Å^2)	U_{33} (Å^2)	U_{eq} (Å^2)[a]
$LaZn_{0.663(5)}As_2$								
La	4*e*	0	0	0.11426(2)	0.0084(2)	0.0084(2)	0.0146(2)	0.0105(2)
Zn[b]	4*d*	0	1/2	1/4	0.0264(7)	0.0264(7)	0.0132(7)	0.0220(6)
As1	4*e*	0	0	0.32565(4)	0.0083(3)	0.0083(3)	0.0171(4)	0.0112(2)
As2	4*c*	0	1/2	0	0.0461(7)	0.0143(5)	0.0116(4)	0.0240(3)
$SmZn_{0.641(3)}As_2$								
Sm	2*c*	1/4	1/4	0.22840(3)	0.0088(1)	0.0088(1)	0.0094(2)	0.0090(1)
Zn[b]	2*b*	3/4	1/4	1/2	0.0264(5)	0.0264(5)	0.0081(5)	0.0203(4)
As1	2*c*	1/4	1/4	0.65937(6)	0.0084(2)	0.0084(2)	0.0124(3)	0.0097(2)
As2	2*a*	3/4	1/4	0	0.0118(2)	0.0118(2)	0.0083(2)	0.0106(2)

[a] U_{eq} is defined as one-third of the trace of the orthogonalized U_{ij} tensor; $U_{12}=U_{13}=U_{23}=0$.
[b] Refined occupancies for the Zn sites are shown in the formulas.

Design 9 T-PPMS dc magnetometer/ac susceptometer. (A measurement made on the Sm-containing sample was deemed unreliable because it contains small amounts of impurity phases.) Susceptibility values were corrected for contributions from the holder and sample diamagnetism.

3. Results and discussion

3.1. Crystal structure

The ternary rare-earth zinc arsenides $RE\mathrm{Zn}_{0.67}\mathrm{As}_2$, previously known for only the Pr member [6], has now been expanded to include RE=La, Ce, Nd, Sm. However, $\mathrm{LaZn}_{0.67}\mathrm{As}_2$ adopts the SrZnBi_2-type structure [27], in contrast to the remaining compounds $RE\mathrm{Zn}_{0.67}\mathrm{As}_2$ (RE=Ce–Nd, Sm), which adopt the HfCuSi_2-type structure [1] (Fig. 1). The SrZnBi_2-type structure is closely related to the HfCuSi_2-type structure except that the c-axis is doubled. Both tetragonal structures consist of a stacking of anionic layers of edge-sharing ZnAs_4 tetrahedra separated from square nets of As atoms by the intervening RE cations. With respect to the stacking c-direction, the $[\mathrm{ZnAs}_{4/4}]$ layers are shifted relative to each other in $\mathrm{LaZn}_{0.67}\mathrm{As}_2$, whereas they are in perfect registry in $RE\mathrm{Zn}_{0.67}\mathrm{As}_2$ (RE=Ce–Nd, Sm). A consequence of this difference in the layer stacking is that the nets of RE atoms are also oriented differently above and below the square net of As atoms. In both structures, the RE atoms are coordinated by eight As atoms in square antiprismatic geometry, with RE–As distances that reflect the diminishing size of the RE on progressing from $\mathrm{LaZn}_{0.67}\mathrm{As}_2$ (3.1080(6)–3.1358(7) Å) to $\mathrm{SmZn}_{0.67}\mathrm{As}_2$ (3.0156(4)–3.0373(3) Å). A simple rationalization can be made for the adoption of two different structure types by noting the disposition of these RE-centered square antiprisms on opposite sites of the square net of As atoms. In $\mathrm{LaZn}_{0.67}\mathrm{As}_2$, this square net lies on a mirror plane, so that a pair of La atoms centered within square antiprisms (which share a common face) are separated by a distance of $d(\mathrm{La}\cdots\mathrm{La})$=4.692(1) Å. Consistent with Pauling's third rule in which the occurence of shared faces in connected polyhedra tends to be avoided [31], substitution with a smaller RE atom would be disfavored. Thus, in $\mathrm{SmZn}_{0.67}\mathrm{As}_2$ (as well as the Ce–Nd members), the square As net lies on an n-glide plane, so that the square antiprisms share common edges and a pair of Sm atoms are separated by a much longer distance of $d(\mathrm{Sm}\cdots\mathrm{Sm})$=5.394(1) Å. The delineation between a SrZnBi_2-type structure for the La member and a HfCuSi_2-type structure for smaller RE members is also observed in $RE\mathrm{Cu}_{1+x}\mathrm{As}_2$ [16] and $RE\mathrm{AuAs}_2$ [9].

The termination of the arsenide series $RE\mathrm{Zn}_{1-x}\mathrm{As}_2$ at RE=Sm seems to run counter to the trend in the extent of RE substitution in the analogous antimonides ($RE\mathrm{Zn}_{1-x}\mathrm{Sb}_2$; RE=La–Nd, Sm, Gd, Tb) [23] and bismuthides ($RE\mathrm{Zn}_{1-x}\mathrm{Bi}_2$; RE=La, Ce, Pr) [24]. This observation can be attributed to crystal chemical factors that influence the degree of distortion in the Zn-centered tetrahedra, which are oriented with their $\bar{4}$-axes parallel to the c-direction. Along this direction, the tetrahedra are always elongated in $RE\mathrm{Zn}_{1-x}\mathrm{As}_2$ and $RE\mathrm{Zn}_{1-x}\mathrm{Sb}_2$ (the four θ_1-angles are larger than the two θ_2-angles), whereas they are compressed in $RE\mathrm{Zn}_{1-x}\mathrm{Bi}_2$ (the four θ_1-angles are smaller than the two θ_2-angles), with the angles defined as shown in Fig. 2. This difference can be understood in an alternative way: through the connection of the [ZnPn] layers to the Pn square nets via the RE atoms (Fig. 1), simple geometric considerations dictate that the top or bottom edge of a ZnPn_4 tetrahedron equal the diagonal in a Pn_4 square, $2d_{\mathrm{Zn}-Pn}\sin(\theta_2/2)=\sqrt{2}d_{Pn-Pn}$, which also corresponds to unit cell edge length a. To maintain the observed Zn–Pn (2.55–2.56, 2.71–2.72, and 2.73–2.76 Å) and Pn–Pn distances (2.79–2.88, 3.01–3.10, and 3.22–3.25 Å), for Pn=As, Sb, and Bi, respectively, it is clear that the tetrahedra must distort from ideality. If θ_2 is chosen to be the ideal tetrahedral angle of 109.5°, the tetrahedron edge length is greater than the square diagonal in the arsenides (4.2 vs. 4.0 Å) or antimonides (4.4 vs. 4.3 Å), whereas the reverse is true for the bismuthides (4.5 vs. 4.6 Å). Thus θ_2 must be less than 109.5° in the arsenides or antimonides, but greater than 109.5° in the bismuthides. When the RE component is now considered, substitution with a smaller RE in the arsenide series tends to exacerbate this distortion to the point where the deviation from ideal tetrahedral angles in the ZnPn_4 tetrahedra becomes quite severe at the Sm member (Fig. 2). (The case of $\mathrm{PrZn}_{1-x}\mathrm{Bi}_2$ involves a splitting of Bi sites as a response to the distortion [24].)

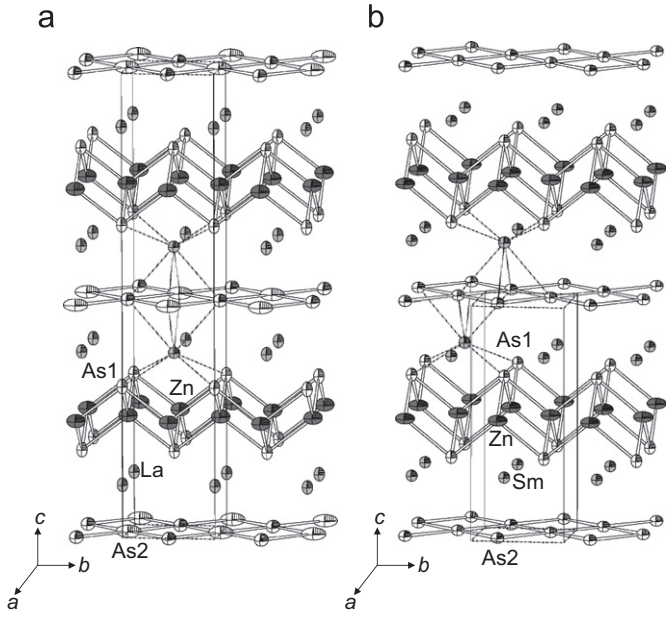

Fig. 1. (a) $\mathrm{LaZn}_{1-x}\mathrm{As}_2$ with SrZnBi_2-type and (b) $RE\mathrm{Zn}_{1-x}\mathrm{As}_2$ (RE=Ce–Nd, Sm) with HfCuSi_2-type structures.

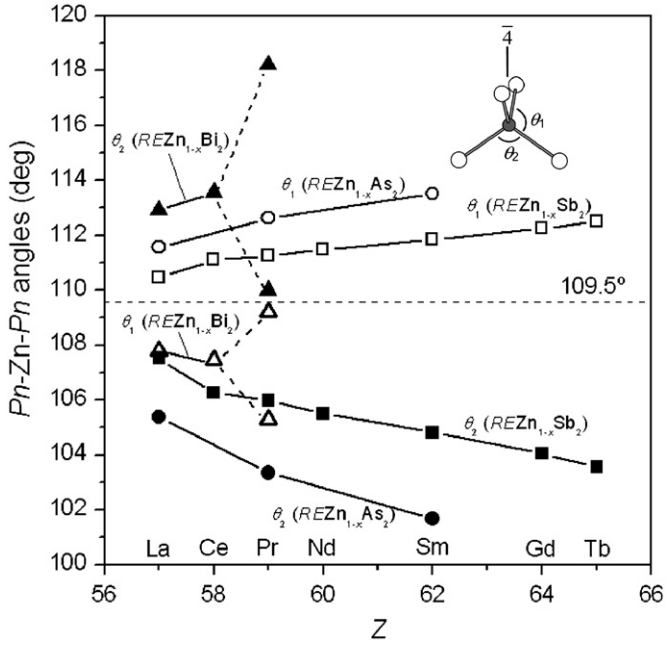

Fig. 2. Plot of Pn–Zn–Pn angles within the ZnPn_4 tetrahedron distorted along the $\bar{4}$-axis in $RE\mathrm{Zn}_{1-x}Pn_2$ (Pn=As, Sb, Bi). Data for the antimonides and bismuthides are taken from previous studies [23,24].

3.2. Electronic structure

The hard-sphere model implicit in the discussion above serves as a starting point to evaluate the electronic structure of $RE\mathrm{Zn}_{1-x}\mathrm{As}_2$. In the usual approach in which the Zintl–Klemm concept is applied, the assumption of full transfer of valence electrons from the electropositive to electronegative components leads to the formulation $(RE^{3+})(\mathrm{Zn}^{2+})_{0.67}(\mathrm{As1}^{3-})(\mathrm{As2}^{1.33-})$, in which the isolated As1 atoms are fully reduced whereas the As2 atoms are not, as manifested by the development of weak homoatomic As–As bonding (2.8–2.9 Å) within the square net of As2 atoms. The ideal electron count for such atoms in square nets is $6e^-$, resulting in a charge of $1-$ for pnicogen atoms participating in so-called "one-electron" *Pn*–*Pn* hypervalent bonding [32]. It is interesting to note that the observed compositions in $RE\mathrm{Zn}_{1-x}Pn_2$ are essentially fixed, with no evidence of significant homogeneity range, but the Zn occupancy tends to decrease as seen, for example, in the progression $\mathrm{LaZn}_{0.67}\mathrm{As}_2$, $\mathrm{LaZn}_{0.61}\mathrm{Sb}_2$ [23], and $\mathrm{LaZn}_{0.52}\mathrm{Bi}_2$ [24], corresponding to charges of $\mathrm{As}^{1.33-}$, $\mathrm{Sb}^{1.22-}$, and $\mathrm{Bi}^{1.04-}$, respectively, for the pnicogen atoms in the square nets. This trend is consistent with the expectation for diminished charge transfer to take place as the pnicogen becomes less electronegative.

An explanation for the partial Zn occupancy can also be sought in terms of optimizing covalent bonding interactions as evaluated from a band structure calculation on an idealized "LaZnAs_2" model with the SrZnBi_2-type structure. In the density of states

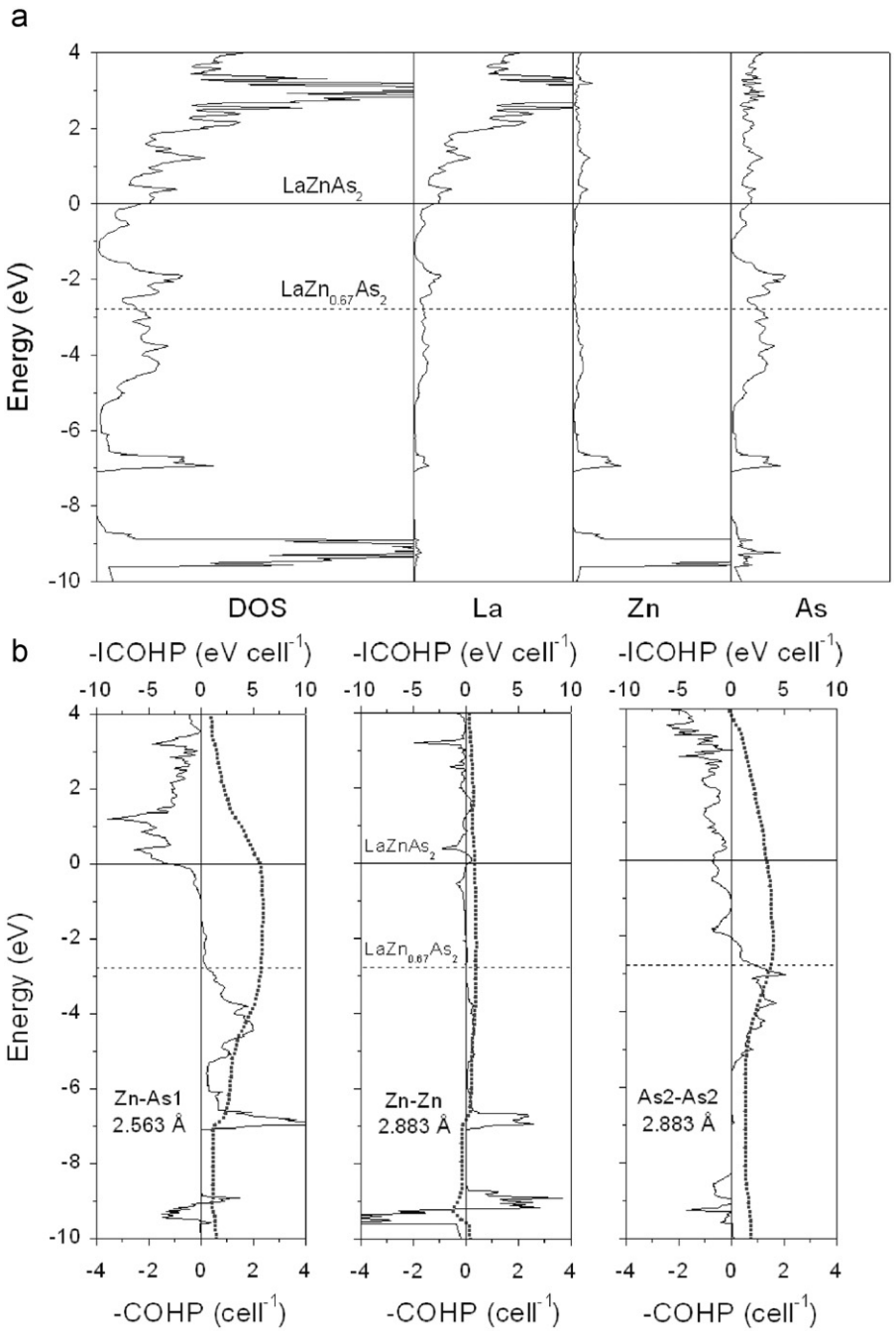

Fig. 3. (a) Density of states (DOS) and its La, Zn, and As projections for $\mathrm{LaZn}_{1-x}\mathrm{As}_2$ (SrZnBi_2-type). (b) Crystal orbital Hamilton population (COHP) (solid lines) and integrated COHP curves (dotted lines) for Zn–As1, Zn–Zn, and As2–As2 interactions. The Fermi level is marked by the solid horizontal lines at 0 eV for the idealized composition "LaZnAs_2" and by the dashed horizontal lines at -2.7 eV for the observed composition "$\mathrm{LaZn}_{0.67}\mathrm{As}_2$".

(DOS) curve, the Fermi level (at 0 eV) lies above a pseudogap near −1 eV, above which are mostly La-based states and below which are mostly Zn- and As-based states (Fig. 3a). The crystal orbital Hamilton population (COHP) curves reveal that Zn–As1, Zn–Zn, and As2–As2 interactions are all antibonding just below 0 eV (Fig. 3b). At the decreased electron count corresponding to "$LaZn_{0.67}As_2$", the Fermi level is lowered to −2.7 eV such that these antibonding states are depopulated. The integrated COHP values (–ICOHP) are changed to reflect strengthened bonding (from 1.40 to 1.43 eV for Zn–As1; from 0.19 to 0.24 eV for Zn–Zn; from 0.82 to 0.94 eV for As2–As2), the most important contribution arising within the square net of As2 atoms. The optimum location of the Fermi level should really be at –2 eV, where bonding and antibonding levels are clearly demarcated, but this analysis neglects the loss of Zn–As (and weak Zn–Zn) contacts that would ensue when Zn sites are vacated. Moreover, local distortions around these vacancies may also take place.

We also performed band structure calculations (not shown) on a "$LaZnAs_2$" model adopting a hypothetical $HfCuSi_2$-type structure in attempts to gain insight for why the $SrZnBi_2$-type structure is experimentally observed instead. Inspection of these crystal structures (Fig. 1) shows that the key differences are the coordination environment around the As2 atom (four La atoms in square planar geometry in $SrZnBi_2$-type vs. tetrahedral geometry in $HfCuSi_2$-type) and the La···La interactions on opposite sites of the square net as described earlier. The different coordination environment around As2 is inconsequential (the La–As2 interactions have identical –ICOHP values of 0.80 eV in both models). The 4.69 Å La···La contact in the $SrZnBi_2$-type model corresponds to very weak bonding (–ICOHP of 0.17 eV) whereas the much longer 5.51 Å La···La contact in the hypothetical $HfCuSi_2$-type model is nonbonding (–ICOHP of 0.00 eV). Although the $SrZnBi_2$-type model is found to be more stable (by 14 kJ/mol) than the $HfCuSi_2$-type model, in agreement with the experimental occurrence of only the former, we advise some skepticism in this explanation because it considers only covalent bonding contributions and neglects the role of Madelung (ionic) contributions.

3.3. Physical properties

Magnetic susceptibility measurements on $REZn_{0.67}As_2$ (RE=Ce, Pr, Nd) reveal unremarkable paramagnetic behavior (Fig. 4), with no hint of a downturn indicative of long-range antiferromagnetic ordering as often observed in related compounds such as $RECuAs_2$ [18–21]. The inverse magnetic susceptibility curves were fit in the region from 50 to 300 K to the Curie–Weiss law, $\chi = C/(T-\theta_p)$. The Weiss parameters θ_p are all negative (−3.8, −4.0, and −9.1 K, respectively), indicating antiferromagnetic exchange interactions. The effective magnetic moments μ_{eff} derived from this fitting are 2.63(1), 3.80(1), and 3.83(1) μ_B for the Ce, Pr, and Nd compounds, respectively, slightly larger but more or less in good agreement with the expected values (2.54, 3.58, and 3.62 μ_B, respectively) for trivalent RE^{3+} species. There are also slight departures from linearity in the inverse magnetic susceptibility curves at low temperatures that warrant further investigation. These results can be contrasted with the corresponding antimonides $REZn_{0.6}Sb_2$ [23], which tend to show more pronounced curvature in their inverse magnetic susceptibility curves and effective magnetic moments that are slightly suppressed relative to the free-ion values, suggesting stronger magnetic coupling with the conduction electrons.

The electrical resistivities for single-crystal samples of $LaZn_{0.67}As_2$ and $SmZn_{0.67}As_2$ are remarkable (Fig. 5). The absolute value of the resistivity for $LaZn_{0.67}As_2$ is very high (on the order of Ω cm) and the temperature dependence implies activated behavior arising from an energy gap, which is inconsistent with the

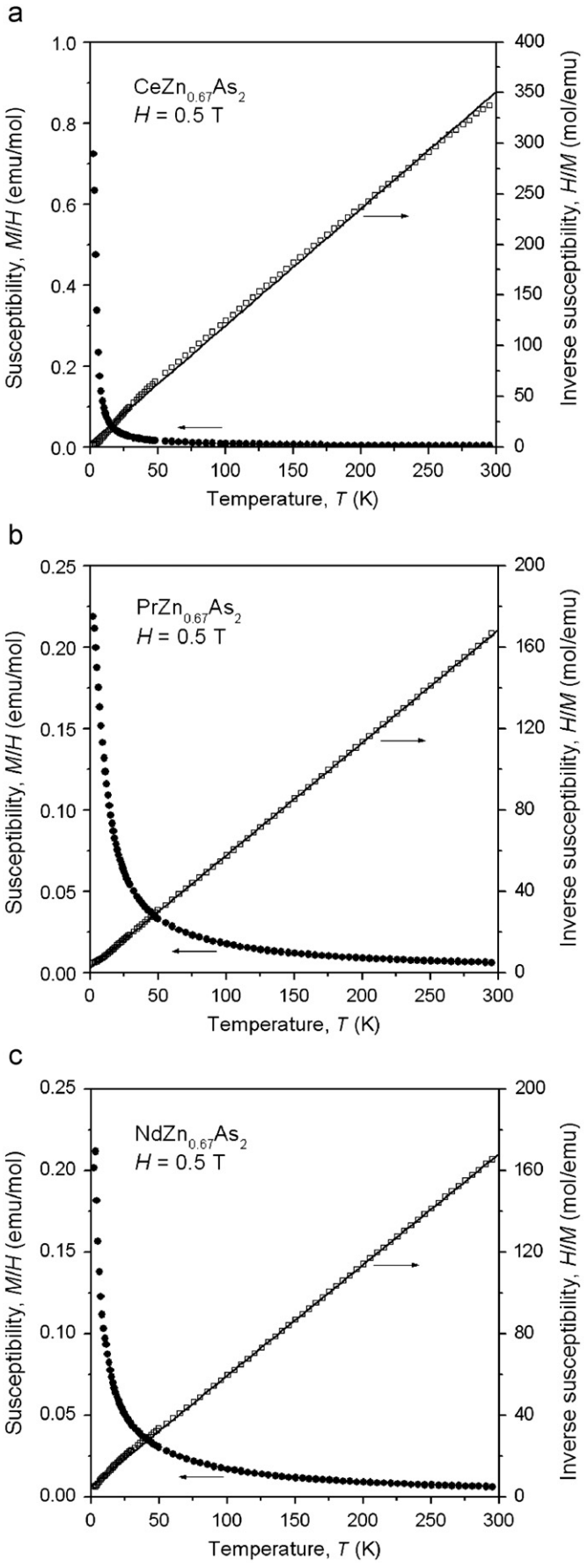

Fig. 4. Plots of magnetic susceptibility (and its inverse) vs. temperature for $REZn_{0.67}As_2$ (RE=Ce–Nd).

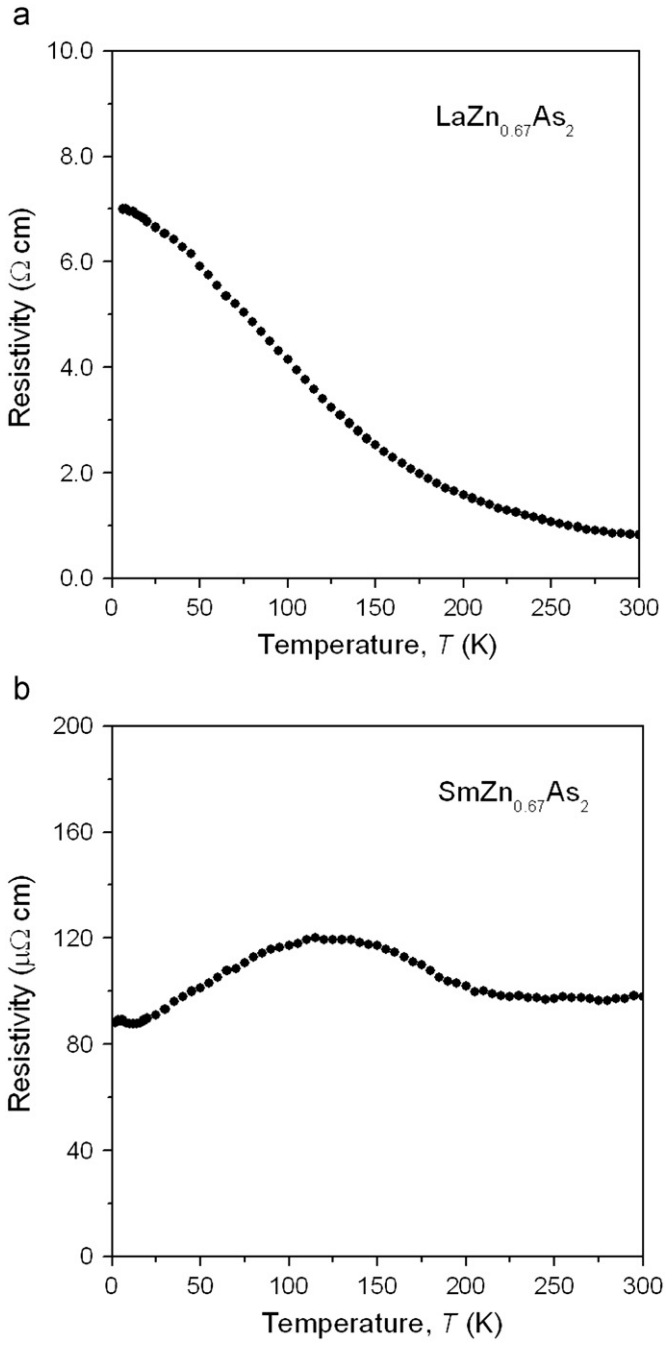

Fig. 5. Plots of electrical resistivity vs. temperature for (a) $LaZn_{0.67}As_2$ and (b) $SmZn_{0.67}As_2$.

position of the Fermi level in the DOS curve corresponding to the electron count for $LaZn_{0.67}As_2$ (Fig. 3a). There is a pseudogap near −1 eV, but placement of the Fermi level there matches with the composition "$LaZn_{0.9}As_2$" instead. Even when a band structure calculation is performed (not shown) on $LaZn_{0.67}As_2$ adopting the ordered superstructure found for $Pr_3Zn_2As_6$ [6], the Fermi level does not fall in an energy gap. The electrical resistivity for $SmZn_{0.67}As_2$ is no less puzzling. Although the absolute value is now in the more typical range for metallic compounds, the temperature dependence is not, following several changes in slope. This behavior is similar to that found in $SmMAs_2$ (M=Cu, Ag, Au), for which characteristic broad minima in the electrical resistivity are also observed; although explanations in terms of conventional models are still elusive, their origin is not believed to be structural but may involve weak magnetic scattering effects [18,22]. It seems likely that the unusual temperature dependences for $LaZn_{0.67}As_2$ and $SmZn_{0.67}As_2$ will have different origins, given that there is no magnetically active species in the former whereas interactions between localized f electrons and conduction electrons are important in the latter.

4. Conclusions

The ternary arsenides $REZn_{1-x}As_2$ adopt average structures corresponding to the $SrZnBi_2$-type (RE=La) or $HfCuSi_2$-type (RE=Ce–Nd, Sm), but it is likely that the square As nets present are subject to distortion leading to a superstructure. Determination of such superstructures is made more difficult because of multiple twinning of crystals. Trends in the RE substitution and the distortion around the $ZnPn_4$ tetrahedra in the related pnictide series $REZn_{1-x}Pn_2$ (Pn=As, Sb, Bi) can be understood readily in terms of geometrical factors in which appropriate Zn–Pn distances must be accommodated while maintaining reasonable Pn–Pn distances within square nets. The square nets are smallest in the arsenides, leading to pronounced elongation of the $ZnAs_4$ tetrahedra. The occurrence of Zn vacancies, leading to the substoichiometric formula $REZn_{0.67}As_2$, can be rationalized by the need to depopulate mostly Zn–As and As–As antibonding levels. Preliminary measurements of physical properties indicate nominal Curie–Weiss paramagnetism in $REZn_{0.67}As_2$ (RE=Ce–Nd) and unusual temperature dependences of the electrical resistivity in $LaZn_{0.67}As_2$ and $SmZn_{0.67}As_2$ that are typical of the perplexing behavior seen in related rare-earth transition-metal arsenides $REMAs_2$.

Acknowledgments

This work was supported by the Natural Sciences and Engineering Research Council of Canada (NSERC). We thank Dr. Robert McDonald and Dr. Michael J. Ferguson (X-ray Crystallography Laboratory) for assistance with the single-crystal X-ray data collection, and Ms. Christina Barker (Department of Chemical and Materials Engineering) for the EDX analyses.

Appendix A. Supplementary materials

Supplementary data associated with this article can be found in the online version at doi:10.1016/j.jssc.2011.07.002.

References

[1] L.S. Andrukhiv, L.A. Lysenko, Ya.P. Yarmolyuk, E.I. Gladyshevskii, Dopov. Akad. Nauk Ukr. RSR, Ser. A: Fiz.-Tekh. Mat. Nauki 7 (1975) 645–648.
[2] R. Pöttgen, D. Johrendt, Z. Naturforsch. B 63 (2008) 1135–1148.
[3] O.L. Sologub, P.S. Salamakha, in: K.A. Gschneidner Jr., J.-C.G. Bünzli, V.K. Pecharsky (Eds.), Handbook on the Physics and Chemistry of Rare Earths, vol. 33, Elsevier, Amsterdam, 2003, pp. 35–146.
[4] A. Mar, in: K.A. Gschneidner Jr., J.-C.G. Bünzli, V.K. Pecharsky (Eds.), Handbook on the Physics and Chemistry of Rare Earths, vol. 36, Elsevier, Amsterdam, 2008, pp. 1–82.
[5] M. Brylak, M.H. Möller, W. Jeitschko, J. Solid State Chem. 115 (1995) 305–308.
[6] A.T. Nientiedt, W. Jeitschko, J. Solid State Chem. 142 (1999) 266–272.
[7] J.-P. Jemetio Feudjio, Th. Doert, P. Böttcher, Z. Kristallogr.-New Cryst. Struct. 217 (2002) 455–457.
[8] R.O. Demchyna, Yu.B. Kuz'ma, V.S. Babizhetsky, J. Alloys Compd. 315 (2001) 158–163.
[9] M. Eschen, W. Jeitschko, Z. Naturforsch. B 58 (2003) 399–409.
[10] Yu. Mozharivskyj, D. Kaczorowski, H.F. Franzen, J. Solid State Chem. 155 (2000) 259–272.
[11] Yu. Mozharivskyj, D. Kaczorowski, H.F. Franzen, Z. Anorg. Allg. Chem. 627 (2001) 2163–2172.

[12] R. Demchyna, J.P.F. Jemetio, Yu. Prots, Th. Doert, L.G. Akselrud, W. Schnelle, Yu. Kuz'ma, Yu. Grin, Z. Anorg. Allg. Chem. 630 (2004) 635–641.
[13] D. Rutzinger, Th. Doert, M. Ruck, Acta Crystallogr., Sect. B 65 (2009) 519–526.
[14] D. Rutzinger, C. Bartsch, Th. Doert, M. Ruck, Acta Crystallogr., Sect. B 65 (2009) 527–534.
[15] D. Rutzinger, C. Bartsch, M. Doerr, H. Rosner, V. Neu, Th. Doert, M. Ruck, J. Solid State Chem. 183 (2010) 510–520.
[16] M. Wang, R. McDonald, A. Mar, J. Solid State Chem. 147 (1999) 140–145.
[17] J.-P. Jemetio, Th. Doert, O. Rademacher, P. Böttcher, J. Alloys Compd. 338 (2002) 93–98.
[18] E.V. Sampathkumaran, K. Sengupta, S. Rayaprol, K.K. Iyer, Th. Doert, J.P.F. Jemetio, Phys. Rev. Lett. 91 (2003) 036603-1–036603-4.
[19] K. Sengupta, E.V. Sampathkumaran, T. Nakano, M. Hedo, M. Abliz, N. Fujiwara, Y. Uwatoko, S. Rayaprol, K. Shigetoh, T. Takabatake, Th. Doert, J.P.F. Jemetio, Phys. Rev. B 70 (2004) 064406-1–064406-5.
[20] K. Sengupta, S. Rayaprol, E.V. Sampathkumaran, Th. Doert, J.P.F. Jemetio, Physica B 348 (2004) 465–474.
[21] M. Szlawska, D. Kaczorowski, J. Alloys Compd. 451 (2008) 464–466.
[22] K. Mukherjee, E.V. Sampathkumaran, D. Rutzinger, Th. Doert, M. Ruck, J. Phys.: Condens. Matter 21 (2009) 506004-1–506004-8.
[23] O.Ya. Zelinska, A. Mar, J. Solid State Chem. 179 (2006) 3776–3783.
[24] O.Ya. Zelinska, A. Mar, J. Alloys Compd. 451 (2008) 606–609.
[25] S.S. Stoyko, A. Mar, unpublished information.
[26] G.M. Sheldrick, SHELXTL, Version 6.12, Bruker AXS Inc., Madison, WI, 2001.
[27] G. Cordier, B. Eisenmann, H. Schäfer, Z. Anorg. Allg. Chem. 426 (1976) 205–214.
[28] G.M. Sheldrick, CELL_NOW, Bruker AXS Inc., Madison, WI, 2008.
[29] L.M. Gelato, E. Parthé, J. Appl. Crystallogr. 20 (1987) 139–143.
[30] R. Tank, O. Jepsen, A. Burkhardt, O.K. Andersen, TB-LMTO-ASA Program, Version 4.7, Max Planck Institut für Festkörperforschung, Stuttgart, Germany, 1998.
[31] L. Pauling, The Nature of the Chemical Bond, 3rd ed., Cornell University Press, Ithaca, NY, 1960.
[32] G.A. Papoian, R. Hoffmann, Angew. Chem. Int. Ed. 39 (2000) 2408–2448.